Geomech. Geophys. Geo-energ. Geo-resour. (2022) 8:130
https://doi.org/10.1007/s40948-022-00437-8

ORIGINAL ARTICLE

Reservoir characterization of the middle Miocene Kareem sandstones, Southern Gulf of Suez Basin, Egypt

Sherif Farouk · Souvik Sen · John D. Pigott · Mohammad Abdelfattah Sarhan

Received: 14 March 2022 / Accepted: 28 June 2022 / Published online: 18 July 2022

Abstract In this study, we have assessed the petrographical and petrophysical characteristics of the progradational, syn-rift Middle Miocene Rahmi sandstone gas reservoir (Lower Kareem Formation) from the East Matr and Amal hydrocarbon fields, southern Gulf of Suez by integrating sidewall cores and wireline logs. We interpreted a reservoir gas gradient of around 0.09 psi/ft from the downhole pressure measurements. Based on well log-based petrophysical analyses, we interpreted that the Rahmi reservoir in the East Matr field has a 0.10–0.18 v/v total porosity, 0.08–0.14 v/v effective porosity, 0.08–0.17 v/v shale volume along with water saturation ranging between 0.09 and 0.32 v/v. The correlated reservoir in the Amal field is observed to have higher porosities (0.17–0.22 v/v total porosity and 0.15–0.19 v/v effective porosity), although it exhibits higher water saturation (0.38–0.54 v/v). The reservoir consists of very fine to coarse grained, poorly to moderately sorted, subangular to subrounded, poorly cemented and moderately compacted sublithic, subarkosic and arkosic arenites with moderate to good intergranular porosity. Abundant lithic fragments and poor textural maturity of the Rahimi sandstones imply a high energy shoreface depositional environment in close proximity to the hinterland. Porosity reduction is attributed to dolomite cementation, kaolinite, formation of pseudomatrix by mechanical compaction of argillaceous lithics, and quartz overgrowth. Long and concavo-convex intergranular contacts indicate that silica needed for quartz cementation was derived by moderate degree of chemical compaction of the quartz grains. Partial to near-complete dissolution of the labile grains (feldspar and lithics) and dolomite attributed to the reservoir quality improvement. Scattered dolomite cements prevented more severe mechanical and chemical compaction.

Article highlights

- The gas-bearing Rahmi reservoir is composed of sublithic arenite and has poor textural maturity.
- Carbonate and clay cementations are identified as the porosity destroying diagenetic agent.

S. Farouk
Exploration Department, Egyptian Petroleum Research Institute (EPRI), 1 Ahmed El-Zomor Street, Nasr City, Cairo, Egypt

S. Sen
Geologix Limited, Dynasty Building, Wing A, Level 4, Andheri Kurla Road, Andheri (E), Mumbai, Maharashtra 400059, India

J. D. Pigott
School of Geosciences, The University of Oklahoma, Norman, OK, USA

M. A. Sarhan (✉)
Geology Department, Faculty of Science, Damietta University, Damietta 34517, Egypt
e-mail: msarhan@du.edu.eg

- Dissolution of dolomite cement, feldspar and lithic fragments contributed to secondary porosity.
- Studied reservoir has a good porosity range along with low shale volume.
- East Matr field has lower water saturation, compared to the Amal field.

Keywords Diagenesis · Reservoir characterization · Rahmi member · East Matr field · Amal field · Gulf of Suez Basin

1 Introduction

Sandstone reservoir characterization requires assessment of depositional textures (size, shape, and sorting), primary composition, facies architecture (geometry, heterogeneity and continuity controlled by depositional environment, and changes in the relative sea level), and diagenetic alterations. The Gulf of Suez Basin (GOSB) includes more than 80 fields producing oil and gas from Precambrian to Neogene successions. The Miocene sediments hold approximately 60% of the hydrocarbon accumulations in the GOSB, while the remaining is hosted by the Pre-Cenomanian Nubia Formation (Peijs et al. 2012). Numerous geological and geophysical studies on the evolution of the GOSB rifting have been conducted because of the huge amount of exploration data and the presence of well-exposed Miocene syn-rift strata (e.g., Alsharhan 2003; El Nady et al. 2015; Sarhan and Basal 2019; Moustafa and Khalil 2020; Sarhan 2020; Elhossainy et al. 2021; Radwan and Sen 2021a-d; Sarhan 2021a, b). The sandstones of the Middle Miocene Kareem Formation are the primary hydrocarbon-bearing reservoirs in the GOSB which accounts for nearly 23% of the GOSB production. These sandstones have a net pay thickness of 10–200 m, porosity range between 7 and 33%, and permeably between 20 and 730 md (Alsharhan 2003). The Kareem Formation comprises of Rahmi and Shagar members. Rahmi Member comprises of intercalated shales, sandstones, carbonate, and anhydrite. Shagar Member comprises of shales and marls, with thin limestone and sandstone beds. This work focuses on the Rahmi Member sandstones in the East Matr and Amal fields, situated in the southern GOSB. Previous literature from Amal field covers the board geological modeling (El Araby et al. 2009), sequence stratigraphic interpretation (Abd El-Naby et al. 2010), seismic data interpretation (Abuel Ata et al. 2012) and pore pressure evaluation (Ramadan et al. 2019) of the Kareem Formation. Literature lacks in reservoir characterization from the East Matr field.

This study integrates cores and well logs of the Rahmi sandstone to infer the reservoir characteristics which has critical influence on the field development and production. The objectives of this work are to: (i) interpret the petrographic characteristics, (ii) estimate the key petrophysical parameters from wireline logs, (iii) unravel the impact of diagenetic processes on petrophysical properties. Using this integrated approach provides new insights into reservoir characterization of syn-rift shoreface sandstones.

2 Geological settings

The GOSB is a part of the Red Sea rift system, which was formed when the Arabian and African plates separated during the Late Oligocene to Early Miocene (Sarhan et al. 2014; Sarhan 2021a; Radwan and Sen 2021a). The rift is a 300-km-long depression that runs along the NW–SE direction (Alsharhan 2003; Radwan and Sen 2021a–d). A sequence of NW–SE trending clysmic normal faults define its 60 to 80 km width. The array of these faults shifted northwest, affecting the UpperMiocene section underneath the Nile Delta Basin (Sarhan et al. 2014). The GOSB is geologically divided into three tectonic provinces: Ataqa in the north, Gharib, and Amal-Zeit in the southern part. The three provinces are divided by two accommodation faults (hinge zones) with N-NE and S-SW directions (Alsharhan 2003). The Southern province (Amal-Zeit) extends from the Morgan accommodation zone to the mouth of the GOSB, where it merges with the Red Sea. It tilts towards the SW and is dominated by faults that dip to the NE. The studied fields, Amal and East Matr Fields are located in the Amal-Zeit Province at the southern part of the Gulf of Suez provenance (Fig. 1). The stratigraphic section of the GOSB was divided into three rift-associated packages by Barakat (1982): Post-rift, Syn-rift, and Pre-rift. Miocene successions represent one of the most important intervals of the Egyptian stratigraphy, as they correspond to one of the most important sources, reservoirs, and major seal rocks for oil

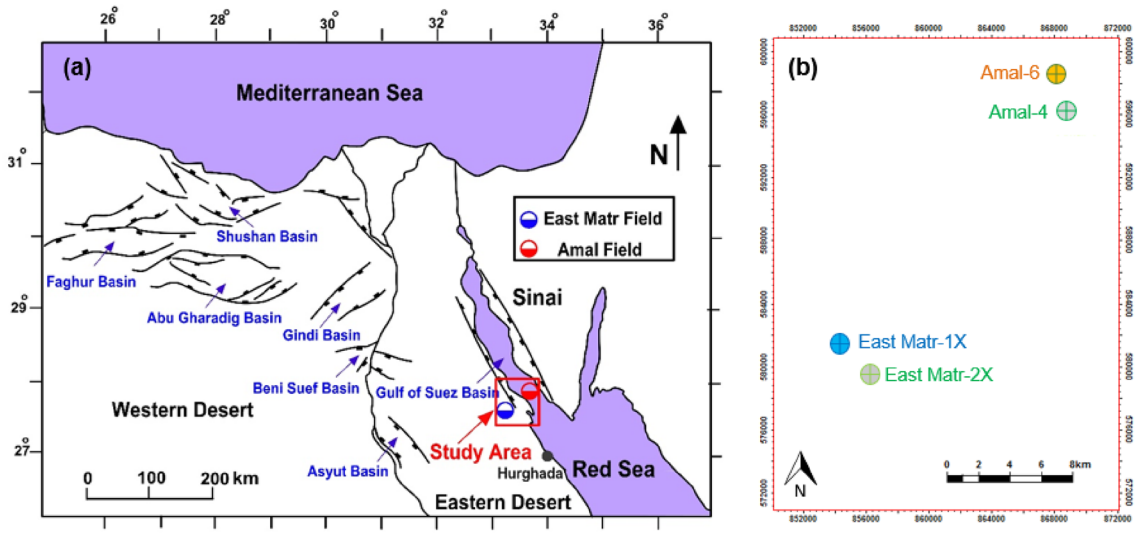

Fig. 1 **a** Location (red square) of the studied East Matr and Amal fields in the southern Gulf of Suez; **b** locations of the studied wells in the two fields

accumulation in the GOSB (Fig. 2). The Middle Miocene age of the Kareem Formation is inferred from the occurrence of *Globorotalia fohsi peripheroronda* and *Cassidulina cruysi* (EGPC, 1964). The Rahmi Member is best represented in the Abu Zenima-1 Well (EGPC, 1974) which exhibits a maximum thickness of 165 m. The unconformable boundary between the Rahmi Member and the underlying Rudeis Formation is inferred from the presence of *Globigerinoides sicanus* and *Operculina complanata* (Youssef 1986), which is marked at the base of the anhydrite interval. The shale and carbonate-bearingShagar Member is best represented in the Gharib North-2 Well which shows a thickness of 297 m (EGPC, 1964). This member lies between Rahmi Member and Belayim evaporites. Langhian to Serravallian age was assigned to Shagar (Youssef 1986) due to the presence of *Globototalia peripheroronda* and *Cassidulina cruysia.*

3 Data and methods

The datasets used in this study include wireline logs from four wells of the East Matr and Amal fields at the southern segment of the GOSB (Fig. 1b). The composite logs for three wells (East Matr-2X, Amal-4 and Amal-6 wells) are also available. Four sidewall core samples were recovered from the Rahmi Member in the well East Matr-2X at 4964 ft, 4965 ft, 4970 ft and 4972 ft. A cumulative of eight thin sections were prepared after vacuum impregnation of the samples with blue epoxy. The samples were examined by scanning electron microscopy technique (SEM). X-ray diffraction (XRD) analysis on the four bulk sidewall core samples provided further information on the whole rock composition and clay fraction.

Due to the unavailability of the core-based petrophysical measurements, we assessed the well-log data from the four studied wells to delineate the potential hydrocarbon-yielding zones within the Rahmi Member of the Kareem Formation. The petrophysical analysis includes the estimation of shale volume, total porosity, effective porosity, water saturation, hydrocarbon saturation and bulk volume of water. **S**hale volume (Vsh) was estimated from gamma ray (GR) and neutron porosity (NPHI) logs. Total porosity (Φt) was calculated using the bulk-density log as proposed by Asquith and Gibson (1982), while effective porosity (Φ_e) was estimated incorporating the effect of Vsh. To estimate water saturation (Sw), we utilized Indonesian model (Poupon and Leveaux 1971):

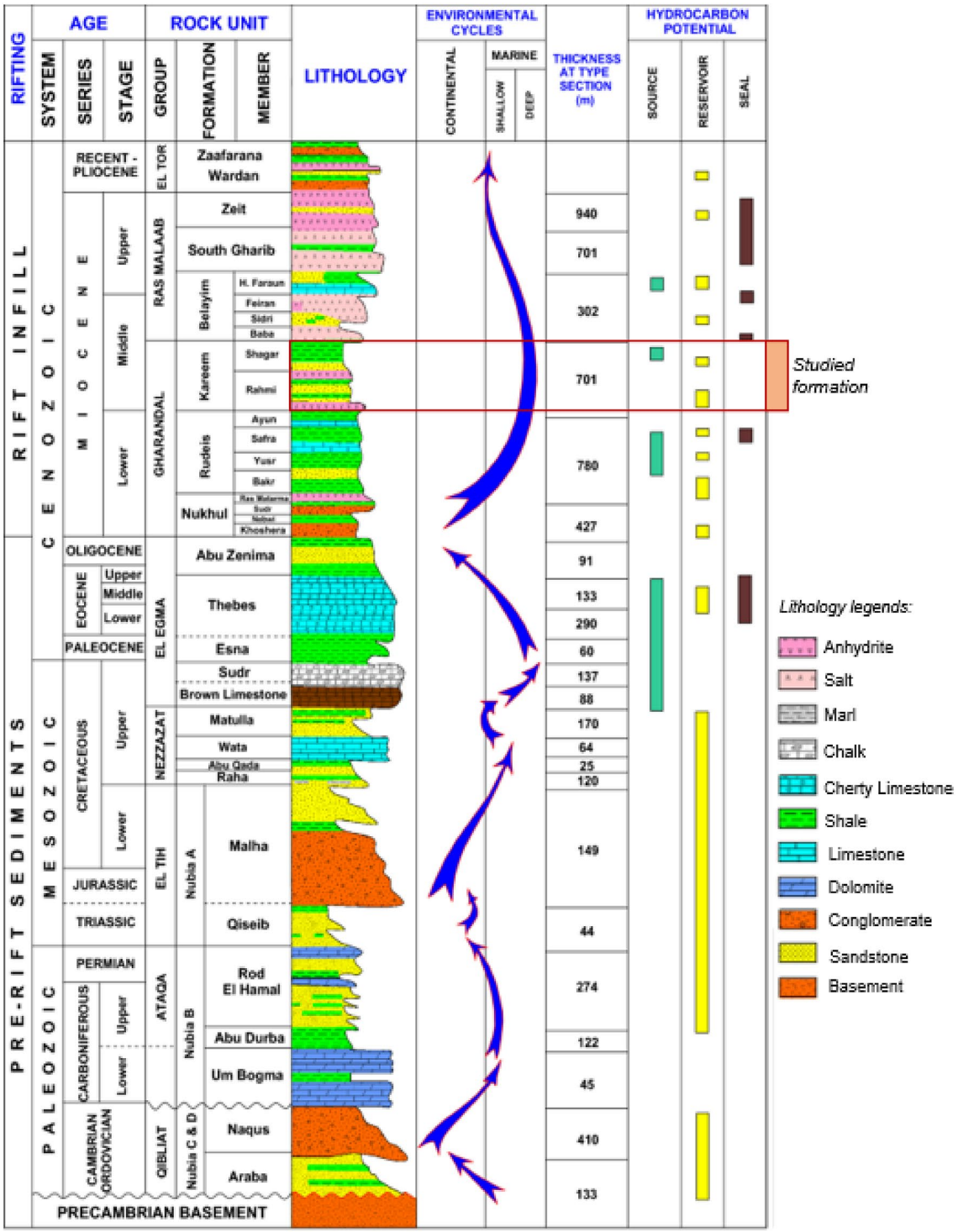

Fig. 2 Stratigraphic column of the Gulf of Suez Basin (GOSB) showing the interval studied, after El Diasty et al. (2020)

$$Sw = \left\{ \frac{\sqrt{\frac{1}{Rt}}}{\left\{ \left(\frac{Vsh^{1-0.5Vsh}}{\sqrt{Rsh}} \right) + \sqrt{\frac{\Phi e^{m}}{aRw}} \right\}} \right\}^{\frac{2}{n}} \quad (1)$$

where, Rsh denotes the resistivity of shale. Rt denotes formation resistivity log, Rw is formation water resistivity, a = tortuosity factor, m and n are cementation and saturation exponents, respectively. Based on the effective porosity and estimated Sw, we have calculated bulk volume of water (BVW) following Buckles (1965):

$$\mathrm{BVW} = \Phi_{e} * \mathrm{Sw} \quad (2)$$

4 Results

4.1 Petrographic investigation

The Rahmi Member sandstones are dominantly composed of monocrystalline and polycrystalline quartz, lithic fragments along with minor amounts of feldspar and bioclasts. The rock fragments include granite, mudstones, sandstones (calcitic and pyritic), dolostone and chert (Figs. 3, 4). The poor to moderately sorted and subangular to subrounded (Figs. 3, 4) detrital grains indicate moderate to low textural maturity of the studied sandstones. Quartz grains display the rare presence of incomplete syntaxial quartz overgrowths. Plagioclase grains, although present in minor abundance, exhibit minor dissolution (Fig. 4c-d). Pore filling pseudomatrix was observed locally in all the sandstone samples (Fig. 3a–b). Authigenic components include mainly ferroan dolomite, calcite, kaolinite and minor illite. Dolomites are the dominant authigenic component and commonly shows various degrees of dissolution (partly to near complete)

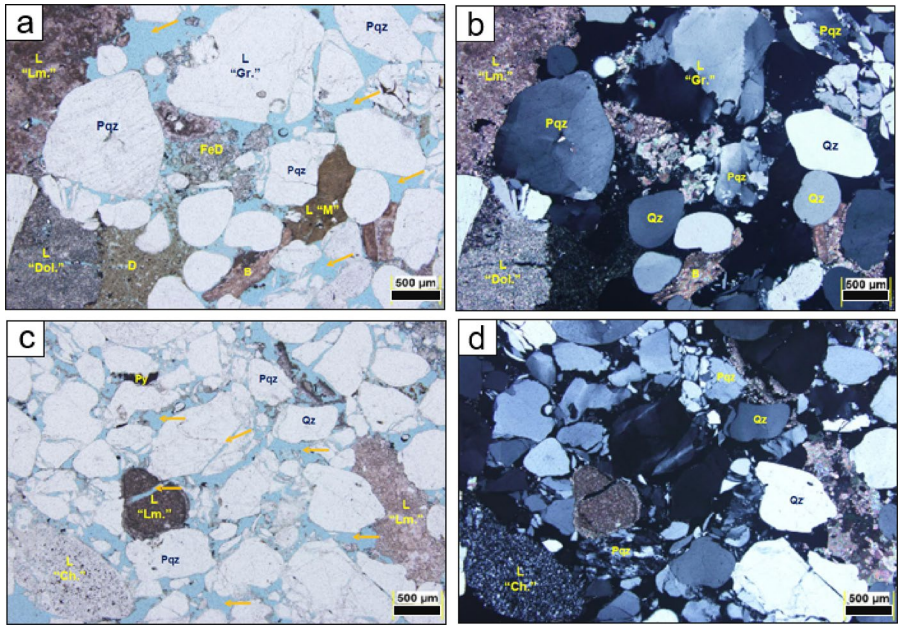

Fig. 3 Optical photomicrographs under plane polar (**a**, **c**) and crossed polar (**b**, **d**) of the studied sandstones showing high amounts of intergranular and smaller amounts of fracture porosity (blue) showing the presence of polycrystalline quartz (Pqz), monocrystalline quartz (Qz), rock fragments of granitic (LGr), chart (LCh), limestone (LLm), dolostone (LDol) and mudstone composition (LM) along with detrital clays (D), partly dissolved ferroan dolostone (FeD) and minor bioclasts (B). Orange arrows indicate pore spaces. Samples belong to depths (**a**–**b**) 4964 ft and (**c**-**d**) 4965.5 ft of the well East Matr-2X

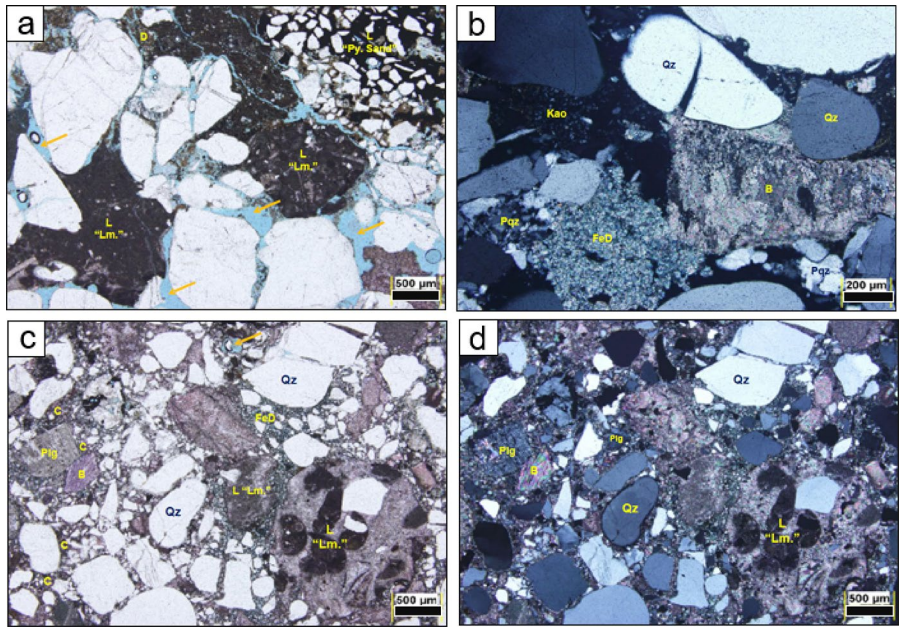

Fig. 4 Optical photomicrographs of the studied sandstones indicating the presence of polycrystalline quartz (Pqz), monocrystalline quartz (Qz), lithic fragments of limestone (LLm), pyritic sandstone (LPy. Sand) along with detrital clays (D), calcite (C), plagioclase feldspar (Plg), partly dissolved ferroan dolomites (FeD), kaolinite (Kao), and minor bioclasts (B), **a** under plane polar, depth 4970 ft; **b** under crossed polar, depth 4970 ft; **c** under plane polar, depth 4972 ft; **d** under crossed polar, depth 4972 ft. Orange arrows indicate pore spaces. Samples belong to the well East Matr-2X

(Fig. 3a–b, 4a–b). Pyrite occurs as disseminated crystals locally filling pore and replacing some of the argillaceous rock fragments. Pore-filling kaolinite (Fig. 4b) ranges in abundances between 0.5% and 4% by volume. The sandstones dominantly contain primary intergranular porosity with good pore connectivity. Average pore sizes range from 20 to 500 µm. Secondary inter-and intraparticle porosity are also commonly observed which are formed due to partial to near-complete dissolution of the labile grains (lithics and feldspars) and dolomite cement. Rare fracture porosity is also observed within detrital grains (mainly quartz) due to overburden pressure (Figs. 3, 4).

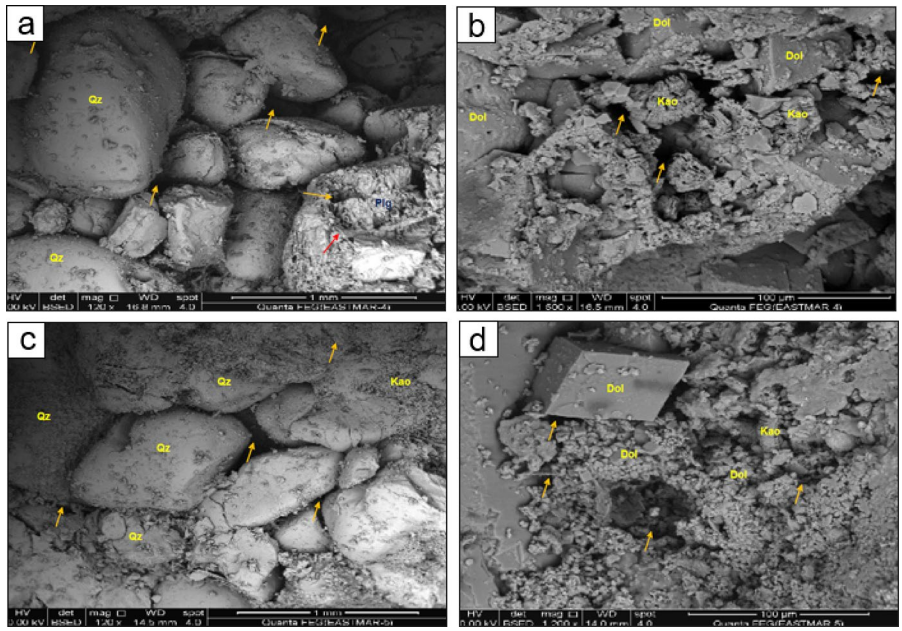

Fig. 5 SEM images showing detrital quartz grains (Qz), pore filling dolomite rhombs (Dol), partly leached to near completely dissolved framework feldspars grains (Plg) and pore filling kaolinite booklets (Kao), red arrow indicates illite, orange arrows indicate pore spaces, (**a**–**b**) depth 4964 ft; (**c**–**d**) depth 4965 ft. Samples belong to the well East Matr-2X

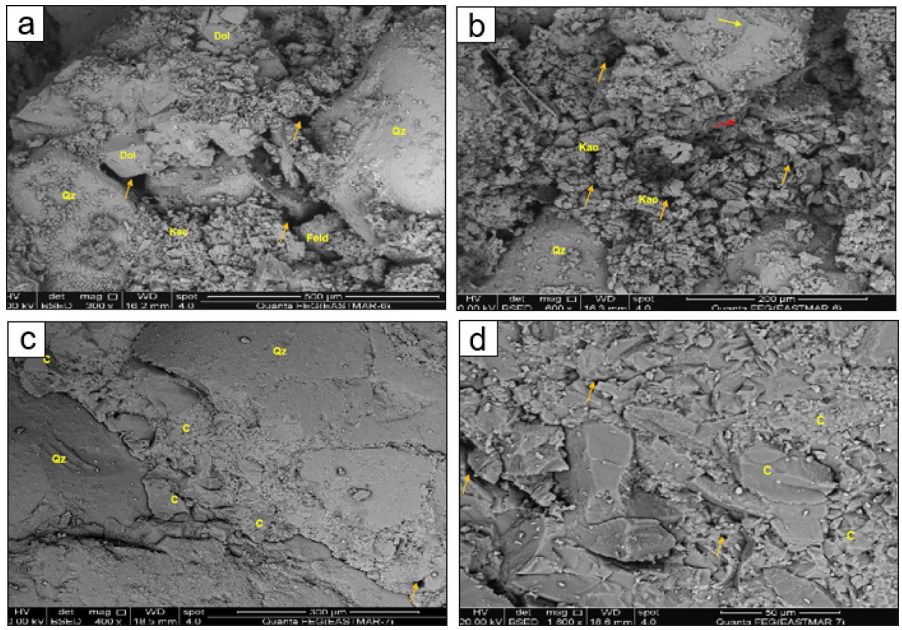

Fig. 6 SEM images showing detrital quartz grains (Qz), pore filling dolomite rhombs (Dol), partly leached to near completely dissolved framework feldspars grains (Plg, or Feld) and pore filling kaolinite booklets (Kao), calcite cement (C), yellow arrows indicate quartz overgrowth, red arrow indicates illite, orange arrows indicate pore spaces, (a-b) depth 4970 ft; (**c**–**d**) depth 4972 ft. Samples belong to the well East Matr-2X

The SEM examinations exhibited the presence of small amounts of slight- to extensively dissolved feldspars grains (Fig. 5a). Rare pore filling and grain coating detrital clay minerals and local pore filling dolomite rhombs were observed (Fig. 5b, d, 6a). Pore filling kaolinite booklets are dominant in all the studied samples, locally showing vermi-from texture of partly corroded pseudohexagonal basal sections (Figs. 5b, d, 6a–b). Hair-like illite occurs in trace quantities (Fig. 6b) as an alteration product of feldspars and replacement of detrital clays. At 4972 ft depth, common pore filling calcite cement is recorded (Fig. 6c-d). XRD results are presented in Fig. 7, which indicates that the quartz and calcite are the dominant minerals (Fig. 7c). Minor to considerable amounts of dolomite, with very minor pyrite and very few amounts of feldspars are locally recorded (Fig. 7c). The dominant clay mineral throughout the analysed samples is kaolinite along with rare amounts of illite (Fig. 7d). Depending on the distribution of the

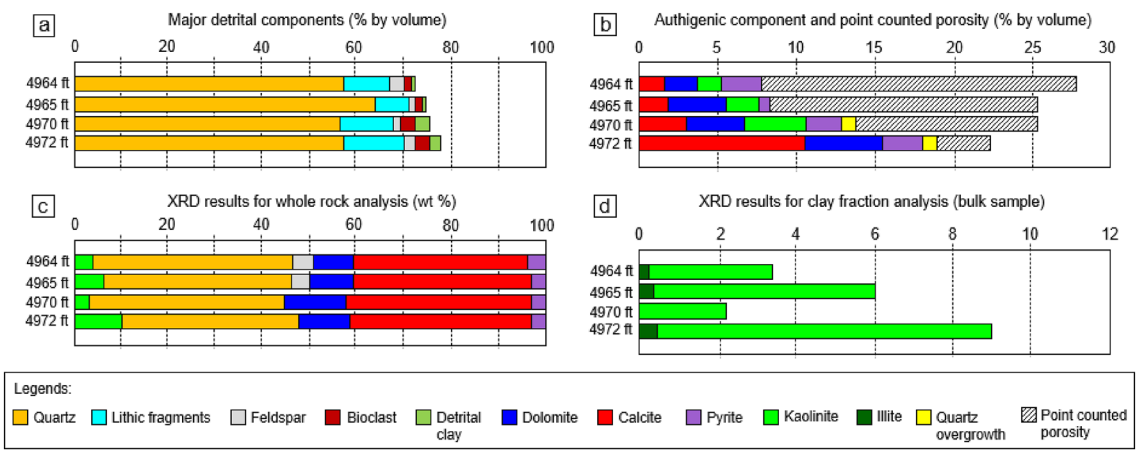

Fig. 7 XRD results of the studied sandstones. **a** major detrital components; **b** authigenic components and point counted porosity; **c** whole rock analysis and **d** clay fraction analysis. Samples belong to the well East Matr-2X

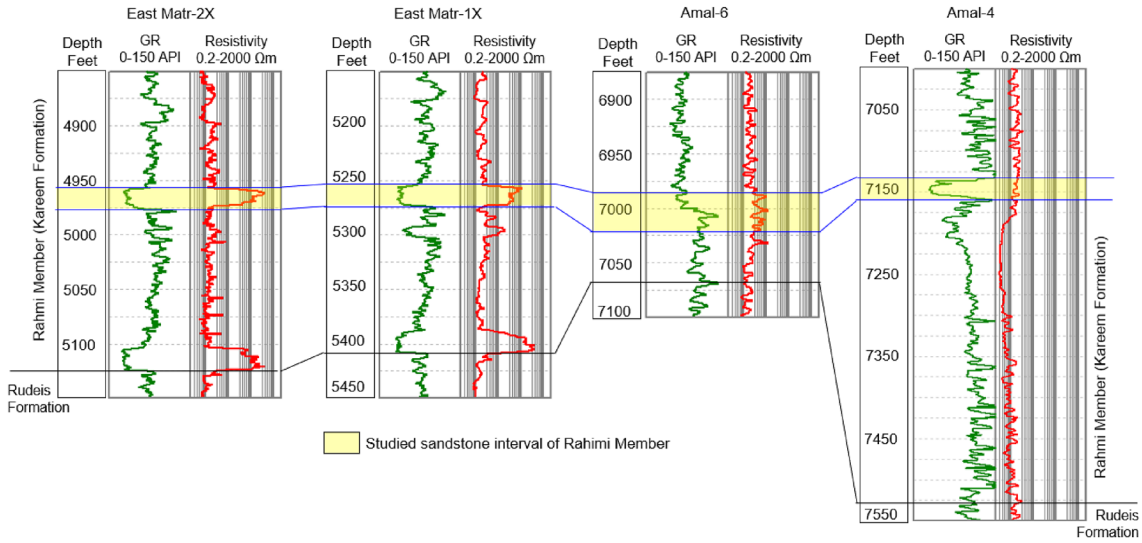

Fig. 8 Wireline log-based correlation of the studied sandstone reservoir of the Rahmi Member (Kareem Formation) between the four studied wells. 'GR' denotes gamma ray log

major detrital constituents (Fig. 7a), the sandstones of the Rahmi Member are inferred as sublithic arenite.

4.2 Petrophysical investigation

The studied sandstone interval of the Rahmi Member of Kareem Formation is correlated in all the studied wells (Fig. 8) based on the low gamma ray and high resistivity signatures. The sandstones of the inspected zones have been described in the composite logs as; colourless, transparent, medium to fine-grained, occasionally coarse-grained, sub-angular to sub-rounded, moderately to poorly sorted with calcareous cement. We utilized neutron porosity-density cross-plots to

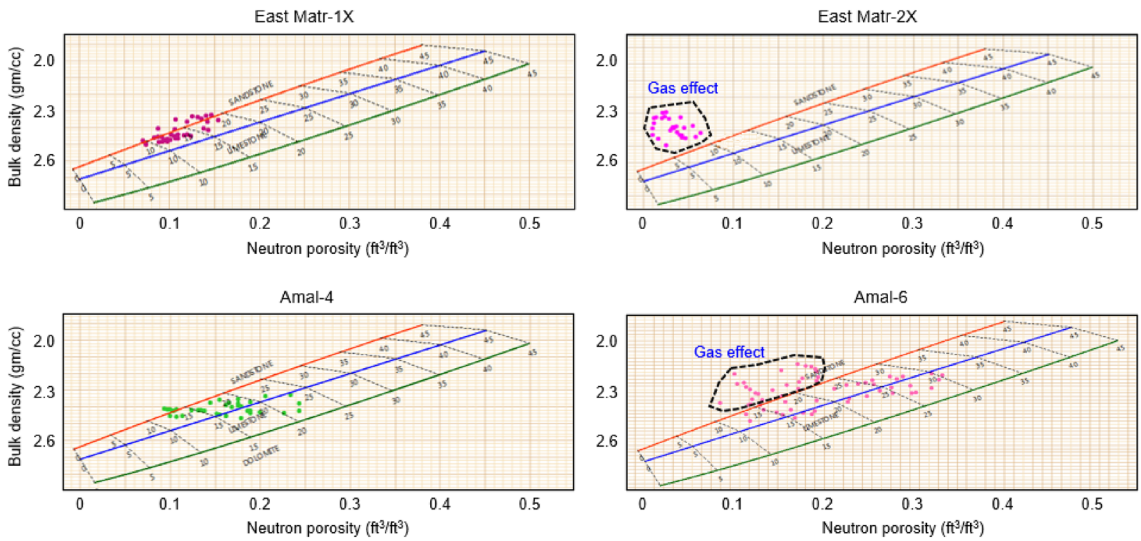

Fig. 9 Cross-plot of neuron porosity versus bulk density indicating lithological composition along with gas effects in the East Matr-2X and Amal-6 wells

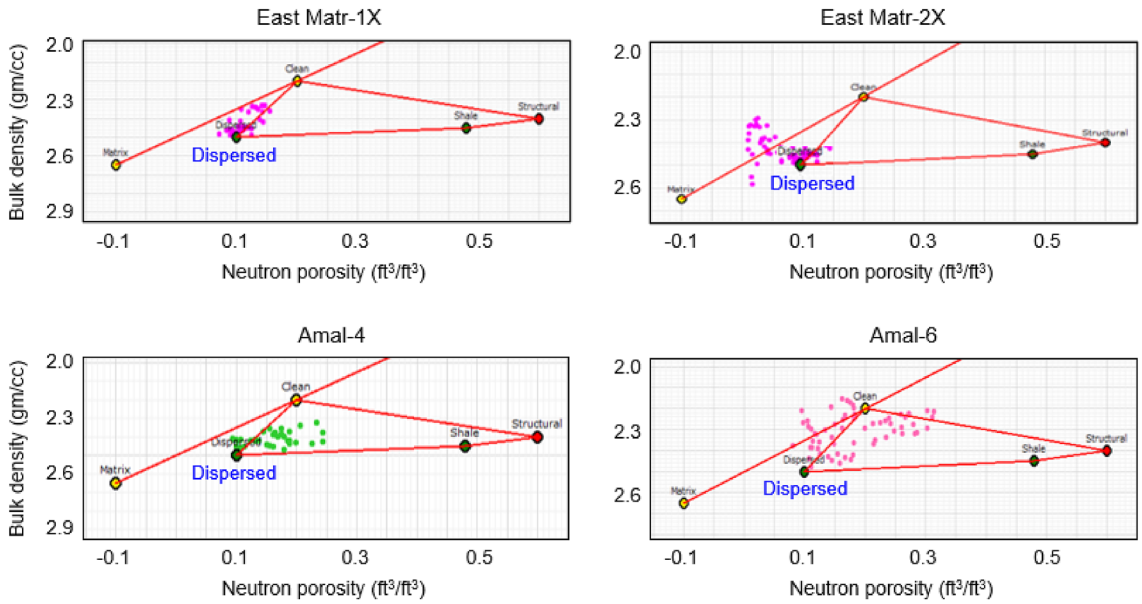

Fig. 10 Thomas Steiber Plot of porosity and bulk density indicating dominantly dispersed clay in all four wells

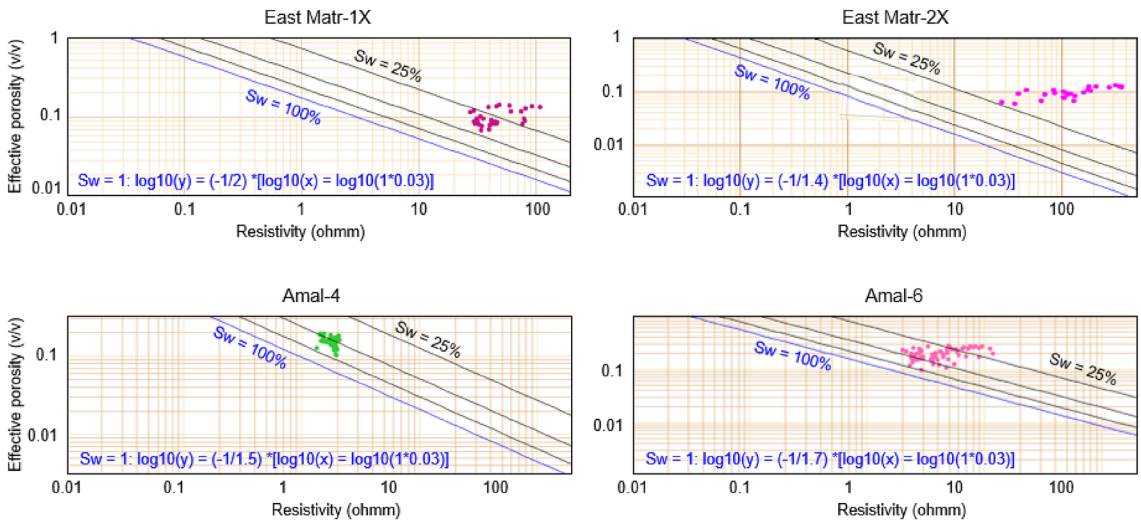

Fig. 11 Pickett plots to decipher the hydrocarbon saturation and input parameters for Sw estimation

confirm the lithology, which also exhibit gas effects in the East Matr-2X and Amal-6 wells (Fig. 9). A porosity and bulk density cross plot (Thomas and Stieber, 1975) indicated dominantly dispersed clay in all four wells (Fig. 10). The Pickett plots (Pickett, 1972) are established for all the studied wells indicating the 100% Sw lines with associated tortuosity factor, cementation and saturation exponents (Fig. 11), which were utilized to determine the water saturation. Sandstone from the East Matr wells plot around and below the Sw = 25% line, confirming that these intervals have the best hydrocarbon potentiality (Fig. 12). However, the majority of the sandstone in the Amal-4 and Amal-6 wells are concentrated around Sw = 50% line indicating lesser hydrocarbon saturation and moderate potential for these pay zones (Fig. 13).

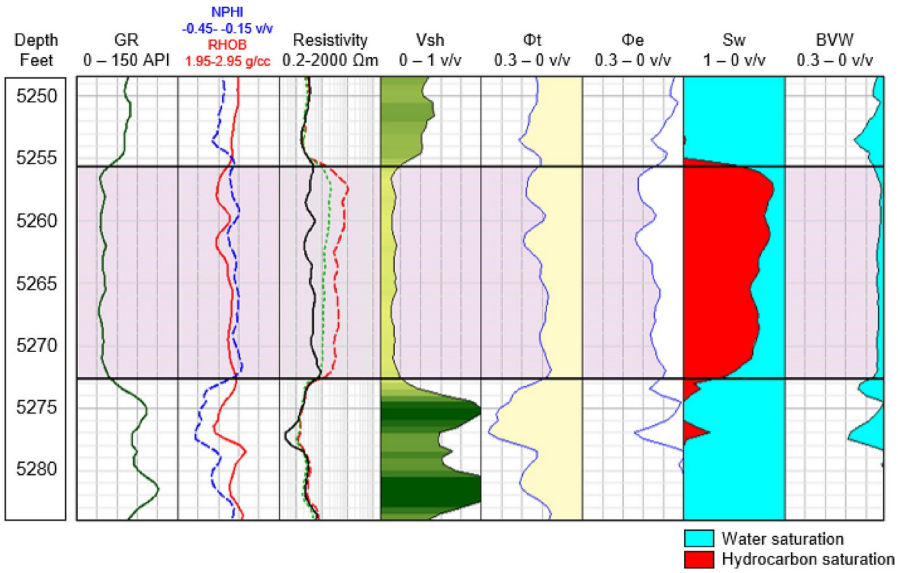

Fig. 12 Petrophysical interpretation of the well East Matr-1X indicating well log-based key petrophysical properties of the Rahmi sandstone interval, Kareem Formation

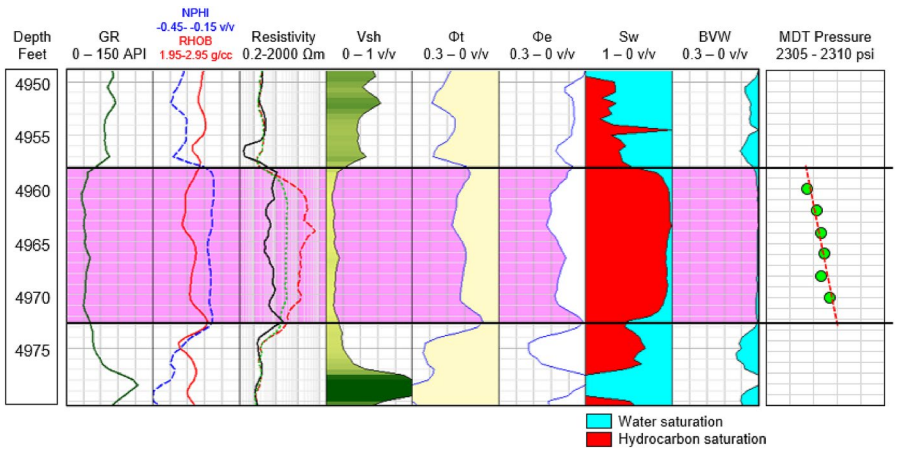

Fig. 13 Petrophysical interpretation of the well East Matr-2X indicating well log-based key petrophysical properties of the Rahmi sandstone interval, Kareem Formation. MDT pressure measurements are plotted on the right-most track. MDT denotes the formation pore pressure measured by Modular Formation Dynamic Tester tool

The quantitative assessment for the target zones in all the four wells encompassing key petrophysical parameters are presented in Figs. 12, 13, 14 and 15. Direct formation pressure measurements available from the well East Matr-2X indicated a pore pressure gradient of 0.09 psi/feet which is representative of gas within the Rahmi sandstone reservoir (Fig. 13). The target sandstone in the well East Matr-1X was encountered between 5256 and 5272 ft and it is characterized by 0.10–0.17 v/v Vsh, 0.10–0.18 v/v Φt, 0.08–0.14 v/v Φe, 0.11–0.32 v/v Sw and 0.02–0.03 BVW (Fig. 12). The same interval was correlated between 4958 and 4972 ft in the well East Matr-2X which exhibits 0.08–0.16 v/v Vsh, 0.11–0.16 v/v Φt, 0.07–0.14 v/v Φe, along with average Sw of 0.09 and BVW value of 0.01 (Fig. 13). In comparison, the wells from the Amal field represent lower Vsh (0.09–0.10 v/v), higher porosities (Φt ~ 0.17–0.22 and Φe ~ 0.15–0.19) associated with higher water saturation (0.38–0.54) and higher BVW (0.06–0.08) (Figs. 14, 15). However, the small ranges of BVW reflect the high-quality hydrocarbon-bearing intervals in the investigated sandstones in both the fields. A comparison of the estimated petrophysical properties (average values) of the Rahmi sandstone interval in all the studied wells is presented in Fig. 16.

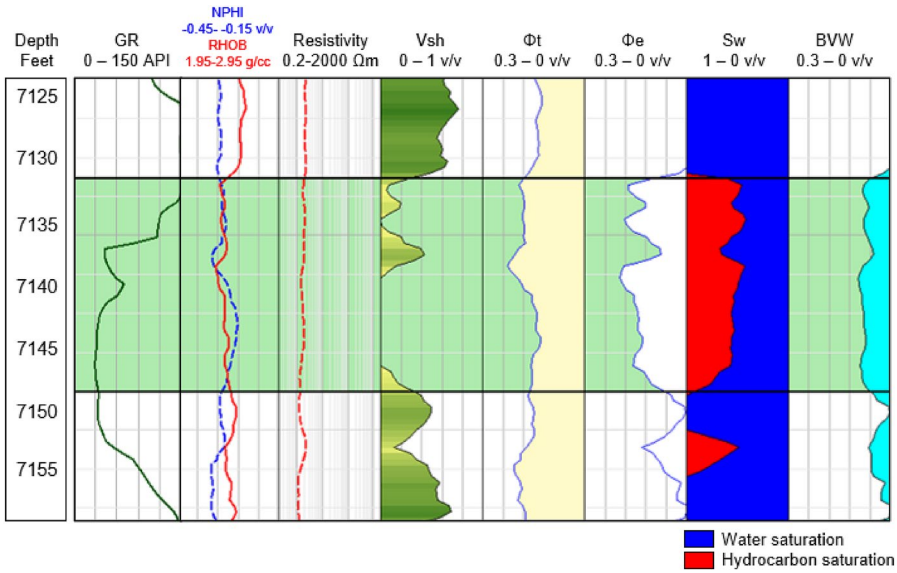

Fig. 14 Petrophysical interpretation of the well Amal-4 indicating well log-based key petrophysical properties of the Rahmi sandstone interval, Kareem Formation

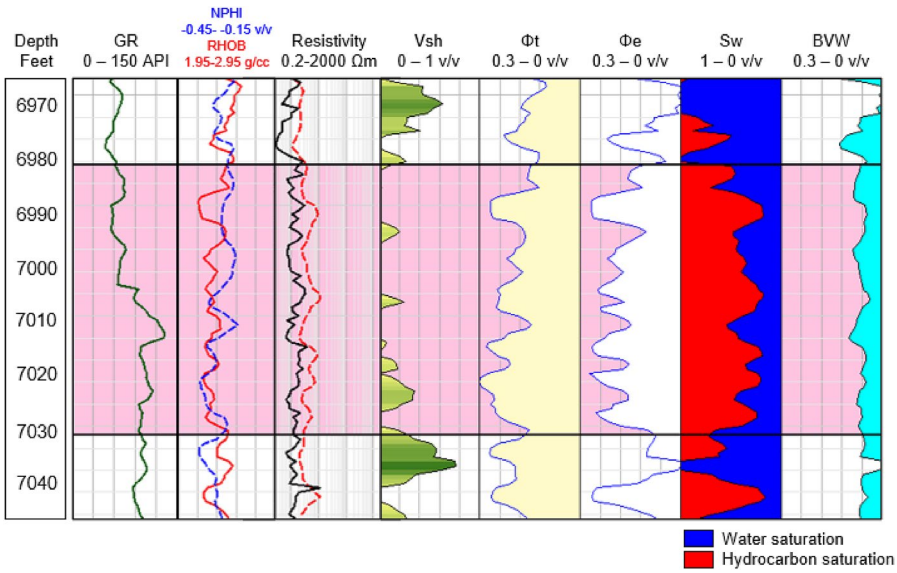

Fig. 15 Petrophysical interpretation of the well Amal-6 indicating well log-based key petrophysical properties of the Rahmi sandstone interval, Kareem Formation

5 Discussions

5.1 Inferences on the depositional environment

Kareem Formation was deposited unconformably over the Lower Miocene Rudeis Formation. The top of Rudeis Formation marks the end of rift climax, above which the Kareem sediments were deposited during late syn-rift (Rohais et al. 2016). A lot of previous works (Tewfik et al. 1992; Salah 1994; Rine et al. 1988; Salah and Alsharhan 1997) inferred alluvial/deltaic fan or submarine fan system responsible for depositing the arkose-quartz arenite sandstones of the Rahmi Member in the southern Gulf of Suez. El Araby et al. (2009) inferred that the medium to coarse grained, poorly sorted lower Kareem sandstones of the Amal field represent proximal fan delta to distal submarine fan where high density currents yielded rapid transportation and deposition of clastic materials. The authors also argued that these coarser clastic beds may represent the base of a Bouma sequence (El Araby et al. 2009). El Sharawy (2013)

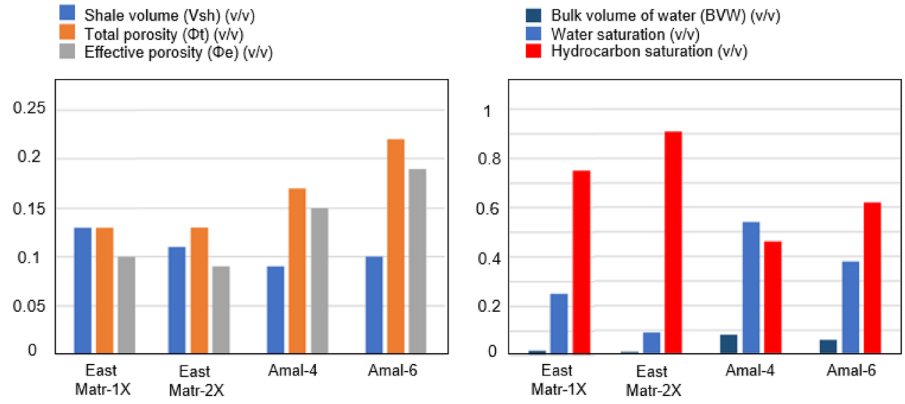

Fig. 16 Comparison of the key petrophysical properties (average values) of the Rahmi sandstone intervals, Kareem Formation in all the studied wells

interpreted the Lower Kareem sands of the southern Gulf of Suez Basin (equivalent to the studied Rahmi Member sandstone) as the basin floor fan (BFF) being deposited during the early phase of relative sea-level fall. The sidewall cores taken out in the well East Matr-2X were too small to look for any sedimentary feature, however they appeared to be massive in nature and devoid of bioturbation. Poor textural maturity (variable grain size, poor sorting and roundness) and abundance of lithic fragments observed in the petrographic analysis, indicate that sedimentation of the Rahmi sandstone had happened in a high energy environment in close proximity of the hinterland (Sen and Dey 2019; Baouche et al. 2020, 2021). This is a typical characteristic of fan deposits (alluvial fans, basin floor fans etc.) (Sen et al. 2016; Dey and Sen 2018; Sen and Dey 2020). Kaolinite, the dominant clay mineral phase in the studied samples, infers their sedimentary origin under continental conditions (Keller 1970; Tsuzuki and Kawabe 1983; De et al. 2020; De and Sengupta 2021; Farouk et al. 2022). The presence of granite, mudstone, sandstone, dolostone and chert rock fragments (Figs. 3–4) provides clues about the source rocks hinterland. During the Miocene period, fan deposits dominated the areas of high relief, which was facilitated by the abundant sediment supply from the older hinterland rocks. Zaid (2013) argued the source areas may have poor vegetation cover as a result of semiarid/arid climate and alluvial fans associated with the rift boundary scarps deposited the Lower Kareem Formation. These fans, documented along the basin periphery, especially in the southern and central margins existed in the close proximity of the Precambrian Basement which acted as the primary sediment source.

5.2 Diagenetic processes affecting Rahmi sandstones

The petrographic investigation of the samples from well East Matr-2X showed that the Rahmi sandstone reservoir was diagenetically altered, which affected the porosity evolution with time, and hence the reservoir potentiality. The early diagenetic history, i.e., eogenesis is characterized by the (i) infiltration of detrital clays (illite etc.) (Figs. 3a, 4a), (ii) rare developments of quartz overgrowth (Fig. 6b), (iii) mild mechanical compaction and (iv) ferroan dolomite formation (early). The later stage of diagenesis, i.e., mesogenesis is characterized by (i) incongruent dissolution of feldspar and lithic fragments (Figs. 4c-d, 5a, 6a), (ii) further fractures by continued mechanical compaction, iii) dolomite formation (late) (Fig. 5b, d), (iv) dissolution of dolomite cements (Fig. 3a-b, 4a-b), (v) calcite cementation (locally significant) (Fig. 6c–d), (vi) precipitation of kaolinite booklets (Figs. 5b, 5d, 6a-b) and vii) formation of pyrites at a much later stage.

Cementation can be very destructive by reducing greater than 50% of reservoir porosity (Worden and Morad 2000; Ganguli et al. 2016; Ganguli, 2017). Clay minerals and carbonate cementations are dominant in the studied sandstones, as seen in the thin sections and SEM. Dolomite cements are abundant in all the thin sections, however they appear to be affected by dissolution (Fig. 3a-b, 4a-b), which enhanced reservoir porosity in the process. Extensive ferroan dolomite cementation is considered to have happened in reducing alkaline pore water conditions (Morad 1998; El-ghali et al. 2009). Authigenic kaolinites, generally, are the products of feldspar dissolution favoured by meteoric water flux of under warm and

humid climatic conditions (Cao et al. 2017; Abdel-Fattah et al. 2022). These kaolinites, occurred as scattered patches and pore filling phases, thus reducing pore throat diameters and have a negative impact on reservoir petrophysical characteristics. Presence of kaolinites indicates that Al and Si bearing minerals (i.e., feldspar etc.) must have been present and the porosity–permeability must have been sufficient to facilitate the migration of acidic pore water to form kaolinites (Zaid et al., 2013). At 4972 ft depth, common pore filling calcite cement is recorded (Fig. 6c-d) which choked the pore spaces. Therefore, calcite cementation can drastically reduce reservoir storage capacity, although it is not dominantly observed in all the samples, so it might be locally significant. Quartz cementation was observed in the studied samples, characterized by minor quartz overgrowths. Overgrowth generally occurs in deep burial diagenetic conditions and favoured by higher temperature (Lai et al. 2017; Worden et al. 2018; Mutebi et al. 2021). Mechanical compaction was inferred based on the concavo-convex detrital grain contacts (Figs. 3, 4) which implies moderate degree of mechanical compaction by burial load.

Dissolution and leaching of the cement and rock constituents are very common in the sandstone reservoirs. These can potentially enhance the potentiality of tight sandstone reservoirs (Lai et al. 2020; Sen et al. 2021; Wang et al. 2021; Farouk et al. 2022). Yuan et al. (2015) and Mosavat et al. (2019) pointed towards the organic acids and CO_2 being the primary agent yielding dissolution in sandstones which might have generated by the thermal evolution of the organic matter. Alternate mechanisms include reverse weathering reaction of silicate minerals under increasing temperature conditions (Hutcheon and Abercrombie 1990) and cooling of high temperature fluids (Giles and De Boer 1989; Taylor 1996) that can also lead to leaching and secondary porosity generation. Bjørlykke (2014) commented that an accurate leaching mechanism generating high volume of secondary porosity is hard to establish. Having said that, dissolution-related secondary porosity is very commonly observed in the sandstone reservoirs and usually produced by the removal of the soluble components such as feldspars, carbonates, authigenic mineral cement, detrital grains, and any soluble minerals (processes classically described by Lindquist 1976; Schmidt et al. 1976; Rowsell and DE Swardt, 1975; Stanton and Mc Bride, 1976). The sandstone dissolution supports the primary pores by creating additional secondary intergranular, intragranular, and vuggy porosity. Dolomite cements, feldspar and lithic fragments appeared to be partially to completely dissolved (Figs. 3a-b, 4–6) which significantly contributed to the secondary porosity network. Darwish and El-Araby (1993) linked the carbonate dissolution in the Kareem sandstones with the late Miocene- Pliocene sea-level fall.

5.3 Inferences on petrophysical characteristics

One of the prominent differences between the log signatures of the East Matr and Amal wells are that the Amal-4 and Amal-6 reservoir zones have much higher gamma ray, i.e., the Rahmi sandstone interval in the well Amal-6 has an average gamma reading of 90 API. Similar observation was also made by Nabawy and El Sharawy (2018), where authors found similar high gamma-ray signatures within the Kareem sandstones in the wells SA-C1 (Shoab Ali Field) and GH375-1 (GH376 Field) of southern Gulf of Suez. Authors reasoned that such behaviour might be contributed by the presence of K-feldspar derived from the unroofing basement rock. El Sharawy (2013) worked on the core-based petrophysical characterization of Kareem sandstones from the Hilal, Sidki, GS365-1 and Amal fields of southern Gulf of Suez. The Kareem sandstone in the wells Amal-9, as interpreted by El Sharawy (2013), contained perthite feldspar (consists of both Na and K-feldspar) which resulted in high gamma ray values against the reservoir. We did not have any thin sections to confirm the dominance of K-feldspar or any potassium-bearing mineral in the studied reservoir from Amal field. However, the kaolinites observed in the East Matr field, are indicative of K-feldspar alteration. Based on the high gamma ray values and available literature, we decipher that the Rahmi sandstones of the Amal field might have more feldspar which experienced a higher degree of dissolution compared to East Matr field and thus resulted in higher total porosity as well as effective porosity (Fig. 16). According to Alsharhan (2003), the reservoir quality of the sandstones of the Kareem Formation is controlled by the variable degrees of diagenetic processes. Nabawy and El Sharawy (2018), based on the core-based porosity and permeability measurements, concluded that the

dolomite content has a negative effect on the reservoir quality of the Kareem sandstones in the Shoab, Hilal GH376, Younis, Nasim and Morgan fields, southern Gulf of Suez. However, in this study, we observed that these dolomite cements are affected by dissolution in the East Matr field contributing to the secondary porosity. El Araby et al. (2009) also documented partly leached to highly altered feldspar grains from the Kareem sandstones of the Amal field (well Amal-10AST). As a summary, cementation and dissolution are interpreted to be porosity reducing and enhancing agents in the studied Rahmi sandstone, respectively. The Rahmi sandstone, in all the studied wells, are characterized by very low shale volume, moderate to good porosity and lower water saturation, which designates the reservoir as a good quality one. The studied gas bearing sandstone interval in the well East Matr-2X yielded promising results during well testing. The well was completed and tested as a gas producer for a flowing period of 3 h at 16/64″ choke which yielded an average 2.4 MMSCFD (million standard cubic feet per day) gas and 113 STBD (stock tank barrel per day) condensate.

6 Conclusions

This study presents the first ever integrated petrophysical and petrographical assessment of the syn-rift Middle Miocene Rahmi gas reservoir from the East Matr and Amal fields. Thin section and SEM-based petrographic investigation of the Rahmi sandstones (Lower Kareem Formation) provided critical information concerning reservoir quality, textural and mineralogical characteristics. A wide range of detrital grain size as well as their poor sorting and angularity reveal short transport distance and quick burial. These sublithic arenites were deposited very close to the faulted and lifted hinterlands, probably as a continental fan deposit during the Middle Miocene late syn-rift stage. Diagenetic processes heavily affected the porosity evolution via cementation and incongruent dissolution of the feldspars. Wireline log-based analysis indicates good porosity ranging between 12 and 22% which consists of both primary intergranular as well as secondary dissolution porosity. A low shale volume indicates that these rift-sands are clean in nature. Lower water saturation (as low as 9%) and BVW infer that the Rahmi sandstones have very good reservoir qualities in both the studied fields.

Acknowledgements We express our sincere gratitude to P.G. Ranjith, Editor-in-Chief, and the anonymous reviewers for their constructive comments that helped the manuscript. We thank the Egyptian General Petroleum Corporation (EGPC) for providing the data utilized in this work.

Funding Open access funding provided by The Science, Technology & Innovation Funding Authority (STDF) in cooperation with The Egyptian Knowledge Bank (EKB). No funding available for this study.

Declarations

Conflict of interest Here, we authorise that there is no conflict of interest.

References

Abd El-Naby AIM, Ghanem H, Boukhary M, Abd El-Aal MH, Luning S, Kuss J (2010) Sequence-stratigraphic interpretation of structurally controlled deposition: middle Miocene Kareem formation, southwestern Gulf of Suez. Egypt Geoarabia 15(3):129–500

Abdel-Fattah MI, Sen S, Abuzied SM, Abioui M, Radwan AE, Benssaou M (2022) Facies analysis and petrophysical investigation of the Late Miocene Abu Madi sandstones gas reservoirs from offshore Baltim East field (Nile Delta, Egypt). Mar Pet Geol 137:105501. https://doi.org/10.1016/j.marpetgeo.2021.105501

Abuel Ata ASA, Azzam SSS, El-Sayed NAA (2012) The improvements of three-dimensional seismic interpretation in comparison with the two-dimensional seismic interpretation in Al-Amal oil field, Gulf of Suez. Egypt Egyptian J Petrol 21:61–69

Alsharhan AS (2003) Petroleum geology and potential hydrocarbon plays in the Gulf of Suez rift basin. Egypt AAPG Bull 87(1):143–180

Araby El A, Moneim AA, Darwish M (2009) Geological modeling of Kareem Formation in Amal oil field, South Gulf of Suez, Egypt. 1st Symposium on the Geological

Resources in the Tethys Realm, Cairo University, March pp. 1–21
Asquith G, Gibson C (1982) Basic well log analysis for geologists: methods in Exploration series. AAPG, Tulsa, Oklahoma.
Baouche R, Sen S, Debiane K, Ganguli SS (2020) Integrated reservoir characterization of the Paleozoic and Mesozoic sandstones of the El Ouar field, Algeria. J Petrol Sci Eng 194:107551. https://doi.org/10.1016/j.petrol.2020.107551
Baouche R, Sen S, Ganguli SS, Feriel HA (2021) Petrophysical, geomechanical and depositional environment characterization of the Triassic TAGI reservoir from the Hassi Berkine South field, Berkine Basin, Southeastern Algeria. J Natural Gas Sci Eng 92:104002. https://doi.org/10.1016/j.jngse.2021.104002
Barakat H (1982) Geochemical criteria for source rock, Gulf of Suez. 6th Egyptian general petroleum corporation. Petrol Exp Prod Conf 1:224–251
Bjørlykke K (2014) Relationships between depositional environments, burial history and rock properties. Some principal aspects of diagenetic process in sedimentary basins. Sed Geol 301:1–14
Buckles RS (1965) Correlating and averaging connate water saturation data. J Can Pet Technol 4(1):42–52
Cao B, Luo X, Zhang L, Sui F, Lin H, Lei Y (2017) Diagenetic evolution of deep sandstones and multiple-stage oil entrapment: a case study from the lower Jurassic Sangonghe formation in the Fukang Sag, Central Junggar basin (NW China). J Petrol Sci Eng 152:136–155
De S, Aastha S (2020) Depositional environment and geomechanical properties of Cambay shale: potential reservoir for shale oil and gas in India. Arab J Geosci 13(12):1–12
De S, Sengupta D (2021) Evaluating the geomechanical properties of Cambay Shale, Cambay Basin, India using advanced wireline logs for shale hydrocarbon exploration. Pet Sci Technol 39(11–12):392–409
Dey J, Sen S (2018) Sequence stratigraphic model of middle Permian Barakar formation from a marginal Gondwana basin. India J Earth Sci 29(4):745–754
Egyptian General Petroleum Corporation Stratigraphic Sub-Committee (EGPC) (1974) Miocene rock stratigraphy of Egypt. Egyptian J Geol 18:1–59
El Sharawy MS (2013) Reservoir characterization of Kareem formation along the central Trough of the Southern Gulf Of Suez. Egypt J Appl Sci Res 9(3):1798–1814
El Diasty WS, El Beialy SY, Mostafa AR, Abo Ghonaim AA, Peters KE (2020) Chemometric differentiation of oil families and their potential source rocks in the Gulf of Suez. Nat Resour Res 29(3):2063–2102
El Nady MM, Ramadan FS, Hammad MM, Lotfy NM (2015) Evaluation of organic matters, hydrocarbon potential and thermal maturity of source rocks based on geochemical and statistical methods: Case study of source rocks in Ras Gharib oilfield, central Gulf of Suez. Egypt Egyptian J Petrol 24(2):203–211
El-ghali MA, Morad S, Mansburg H, Miguel AC, Sirat M, Ogle (2009) Diagenetic alterations to marine transgression and regression in fluvial and shallow marine sandstones of the Triassic Buntsandstein and Keuper sequence, the Paris basin, France. Mar Pet Geol 26:289–309
Elhossainy MM, Salman AM, Sarhan MA, Al-Areeq NM, Alrefaee HA (2021) Sequence stratigraphic analysis and depositional evolution of the upper cretaceous deposits in Ras Budran oil field, Gulf of Suez. Egypt Arab J Geosci 14(12):1–13
Farouk S, Sen S, Abuseda H, El-Shamly Y, Salam A, Elhossainy MM (2022) Petrophysical characterization of the turonian and cenomanian intervals in the Abu Gharadig field, Western desert, Egypt: inferences on reservoir quality and resource development. Nat Resour Res 31:1793–1824. https://doi.org/10.1007/s11053-022-10069-0
Ganguli SS, Vedanti N, Dimri VP (2016) 4D reservoir characterization using well log data for feasible CO2-enhanced oil recovery at Ankleshwar, Cambay Basin – A rock physics diagnostic and modeling approach. J Appl Geophys 135:111–121
Ganguli SS (2017) Integrated reservoir studies for CO2-enhanced oil recovery and sequestration: application to an Indian mature oil field. Springer Thesis Series, Springer International Publishing AG, Germany, p. 181, ISBN: 978–3–319–55842–4
Giles MR, De Boer RB (1989) Secondary porosity: creation of enhanced porosities in the subsurface from the dissolution of carbonate cements as a result of cooling formation waters. Mar Pet Geol 6(3):261–269
Hutcheon I, Abercrombie H (1990) Carbon dioxide in clastic rocks and silicate hydrolysis. Geology 18(6):541–544
Keller WD (1970) Environmental aspects of clay minerals. J Sediment Res 40(3):788–813
Lai J, Wang G, Chai Y, Xin Y, Wu Q, Zhang X, Sun Y (2017) Deep burial diagenesis and reservoir quality evolution of high-temperature, high-pressure sandstones: examples from lower Cretaceous Bashijiqike Formation in Keshen area, Kuqa depression. Tarim Basin of China AAPG Bull 101(6):829–862
Lai J, Fan X, Liu B, Pang X, Zhu S, Xie W, Wang G (2020) Qualitative and quantitative prediction of diagenetic facies via well logs. Mar Pet Geol 120:104486
Lindquist S (1976) Leached porosity in overpressured sandstones-frio formation (Oligocene), South Texas. GCAGS-GC Section SEPM Annual Meeting, Shreveport, Louisiana, USA. AAPG Search and Discovery Article #90975
Morad S (1998) Carbonate cementation in sandstones; distribution patterns and geochemical evolution. In: Morad, S. (Ed.), Carbonate Cementation in Sandstones, vol. 26. International Association of Sedimentologists, (Special Publication), pp. 1–26
Mosavat N, Hasanidarabadi B, Pourafshary P (2019) Gaseous slip flow simulation in a micro/nano pore-throat structure using the lattice Boltzmann model. J Petrol Sci Eng 177:93–103
Moustafa AR, Khalil SM (2020) Structural setting and tectonic evolution of the Gulf of Suez, NW red Sea and Gulf of Aqaba Rift systems. The geology of Egypt. Springer, Cham., pp 295–342
Mutebi S, Sen S, Sserubiri T, Rudra A, Ganguli SS, Radwan AE (2021) Geological characterization of the Miocene-Pliocene succession in the Semliki Basin, Uganda: Implications for hydrocarbon exploration and drilling in the East African Rift System. Natural Resources Research. https://doi.org/10.1007/s11053-021-09951-0

Nabawy BS, El Sharawy MS (2018) Reservoir assessment and quality discrimination of Kareem Formation using integrated petrophysical data, Southern Gulf of Suez. Egypt Marine and Petrol Geol 93:230–246

Egyptian General Petroleum Corporation Stratigraphic Committee (EGPC), 1964. Oligocene and Miocene rock stratigraphy of the Gulf of Suez basin. 142p.

Peijs JAMM, Bevan TG, Piombino JT (2012) The Gulf of Suez rift basin. In: Roberts, Bally (Eds.), Phanerozoic Rift Systems and Sedimentary Basins. Elsevier B.V., pp. 165–194

Poupon A, Leveaux J (1971) Evaluation of water saturation in shaly formations. In SPWLA 12th annual logging symposium. Soc Petrophys Well-Log Anal

Radwan AE, Sen S (2021c) Stress path analysis of the depleted Middle Miocene clastic reservoirs in the Badri field, Gulf of Suez Rift Basin, Egypt. SPE Annual Technical Conference and Exhibition (ATCE), Dubai, UAE, Sept 21–23. SPE-205900

Radwan AE, Sen S (2021d) Stress path analysis of the depleted Miocene clastic reservoirs in the El Morgan field, offshore Egypt. 55th U.S. Rock Mechanics/Geomechanics Symposium (ARMA), Virtual, June 18–25. ARMA-2021d-1346

Radwan A, Sen S (2021a) Stress path analysis for characterization of in situ stress state and effect of reservoir depletion on present-day stress magnitudes: Reservoir geomechanical modeling in the Gulf of Suez Rift Basin. Egypt Natural Resour Res 30(1):463–478

Radwan AE, Sen S (2021b) Characterization of in-situ stresses and its implications for production and reservoir stability in the depleted El Morgan hydrocarbon field, Gulf of Suez Rift Basin. Egypt J Struct Geol 148:104355

Ramadan MAM, Abd El Hamed AG, Bardan F, Nooh AZ (2019) Relation between hydrocarbon saturation and pore pressure evaluation for the Amal Field Area, Gulf of Suez. Egypt Egyptian Journal of Petroleum 28:1–9

Rine JM, Hassouba A et al (1988) Evolution of a Miocene fan delta. In: Nemec W, Steel RJ (eds) a giant oilfield in the Gulf of Suez, Egypt, In: Fan Deltas – sedimentology and tectonic settings. Blackie, pp 239–251

Rohais S, Barrois A, Colletta B, Moretti I (2016) Pre-salt to salt stratigraphic architecture in a rift basin: insights from a basin-scale study of the Gulf of Suez (Egypt). Arab J Geosci 9:317

Rowsell DM, DE Swardt AMJ (1975) Secondary leaching porosity in Middle Ecca sandstones. Trans Geol Soc South Africa 77(2):131–140

Salah MG, Alsharhan AS (1997) The Miocene Kareem Formation in the Southern Gulf of Suez, Egypt: a review of stratigraphy and petroleum geology. J Pet Geol 20(3):327–346

Salah MG (1994) Geology of the northwestern Red Sea with special emphasis on the petrology, sedimentology and hydrocarbon potential of the Miocene Kareem Formation. PhD. Thesis, Cairo University, 166 pp

Sarhan MA (2020) Geophysical appraisal and oil potential for Rudeis Formation at West Hurghada area, southern Gulf of Suez: detection of stratigraphic trap. Arab J Geosci 13(6):1–9

Sarhan MA (2021a) Geophysical and hydrocarbon prospect evaluation of Nukhul formation at Rabeh East oil field, Southern Gulf of Suez Basin. Egypt J Petrol Exp Prod Technol 11(7):2877–2890

Sarhan MA (2021b) Petrophysical characterization for Thebes and Matulla reservoirs in Rabeh East Field, Gulf of Suez Basin, via well logging interpretation. J Petrol Exp Prod Technol 11(10):3699–3712

Sarhan MA, Basal AMK (2019) Evaluation of Nubia sandstone reservoir as inferred from well logging data interpretation for Rabeh East-25 well, Southwest Gulf of Suez. Egypt J African Earth Sci 155:124–136

Sarhan MA, Collier REL, Basal A, Aal MHA (2014) Late Miocene normal faulting beneath the northern Nile Delta: NNW propagation of the Gulf of Suez Rift. Arab J Geosci 7(11):4563–4571

Schmidt v, Mac Donald DA, Platt RL (1976) Pore geometry and reservoir aspects of secondary porosity in sandstones (Abstract). CIM-CSPG Joint Meeting on Enhanced Recovery, pp. 106–107

Sen S, Dey J (2019) A field-scale overview of facies architectures and depositional environment integrating core and geophysical log data: study from a Marginal Gondwana Basin, India. J Geol Soc India 94(3):238–244

Sen S, Dey J (2020) Cyclic sedimentation in the barakar formation of the Karanpura Field, marginal Gondwana Basin, India. J Geol Soc India 95:293–300

Sen S, Das N, Maiti D (2016) Facies analysis and depositional model of Late Permian Raniganj Formation: study from Raniganj coal bed methane block, India. J Geol Soc India 88(4):503–516

Sen S, Abioui M, Ganguli SS, Elsheikh A, Debnath A, Benssaou M, Abdelhady AA (2021) Petrophysical heterogeneity of the early Cretaceous Alamein dolomite reservoir from North Razzak oil field, Egypt integrating well logs, core measurements, and machine learning approach. Fuel 306:121698

Stanton GD, McBride EF (1976) Factors influencing porosity and permeability of lower Wilcox (Eocene) sandstone, Karnes county, Texas (Abstract). AAPG and SEPM Ann Meeting 1:119p

Taylor TR (1996) Association of allochthonous waters and reservoir enhancement in deeply buried Miocene sandstones: picaroon field, Corsair trend, offshore Texas. In: Crossey, L.J., Loucks, R., Totten, M.W. (Eds.), Siliciclastic Diagenesis and Fluid Flow: Concepts and Applications, SEPM Special Publication, 55: 37–48.

Tewfik N, Harwood C, Deighton I (1992) The Miocene, Rudeis and Kareem Formations in the Gulf of Suez: Aspects of sedimentology and geohistory. In: 11th EGPC, Exploration Seminar, Cairo, 1: 84–113

Tsuzuki Y, Kawabe I (1983) Polymorphic transformations of kaolin minerals in aqueous solutions. Geochim Cosmochim Acta 47:59–66

Wang J, Fu Y, Yan Z, Fu J, Xie J, Li K, Zhao Y (2021) Influence of sedimentation and diagenesis on reservoir physical properties: a case study of the Funing formation, Subei Basin, Eastern China. Front Earth Sci 15:892–908

Worden RH, Armitage PJ, Butcher AR, Churchill JM, Csoma AE, Hollis C, Lander RH, Omma JE (2018) Petroleum reservoir quality prediction: overview and contrasting approaches from sandstone and carbonate communities. In: Armitage, P.J., Butcher, A.R., Churchill, J.M., Csoma, A.E., Hollis, C., Lander, R.H., Omma, J.E., Worden, R.H. (Eds.), Reservoir Quality of Clastic and Carbonate Rocks:

Analysis, Modelling and Prediction. Geological Society of London, Special Publications, 435(1), 1–31.

Worden RH, Morad S (2000) Quartz cementation in oil field sandstones: a review of the key controversies. Quartz Cement Sandstones 29:1–20

Youssef A (1986) Coastal to shallow marine Miocene facies in Zeit Bay area, Gulf of Suez, 8th EGPC. Exp Seminar, Cairo 1:344–359

Yuan G, Cao Y, Jia Z, Gluyas J, Yang T, Wang Y, Xi K (2015) Selective dissolution of feldspars in the presence of carbonates: the way to generate secondary pores in buried sandstones by organic CO_2. Mar Pet Geol 60:105–119

Zaid SM (2013) Provenance, diagenesis, tectonic setting and reservoir quality of the sandstones of the Kareem formation, Gulf of Suez. Egypt J African Earth Sci 85:31–52